Journal of Pathology
J Pathol November 2022; **258:** 264–277
Published online 13 September 2022 in Wiley Online Library
(wileyonlinelibrary.com) DOI: 10.1002/path.5997

ORIGINAL ARTICLE

Adrenomedullin2 stimulates progression of thyroid cancer in mice and humans under nutrient excess conditions

Jung Tae Kim[1,2], Mi Ae Lim[3], Seong Eun Lee[1], Hyun Jung Kim[4], Hyun Yong Koh[4], Jeong Ho Lee[4], Sang Mi Jun[5,6], Jin Man Kim[7], Kun Ho Kim[8], Hyo Shik Shin[9], Sun Wook Cho[9,10,11], Koon Soon Kim[1,12], Minho Shong[1,2,12], Bon Seok Koo[2,3]* and Yea Eun Kang[1,12]*

[1] *Research Center for Endocrine and Metabolic Diseases, Chungnam National University School of Medicine, Daejeon, Republic of Korea*
[2] *Department of Medical Science, Chungnam National University School of Medicine, Daejeon, Republic of Korea*
[3] *Department of Otolaryngology-Head and Neck Surgery, Chungnam National University School of Medicine, Daejeon, Republic of Korea*
[4] *Graduate School of Medical Science and Engineering, Korea Advanced Institute of Science and Technology (KAIST), Daejeon, Republic of Korea*
[5] *Center for Research Equipment, Korea Basic Science Institute, Cheongju, Republic of Korea*
[6] *Convergent Research Center for Emerging Virus Infection, Korea Research Institute of Chemical Technology, Daejeon, Republic of Korea*
[7] *Department of Pathology, Chungnam National University School of Medicine, Daejeon, Republic of Korea*
[8] *Department of Nuclear Medicine, Chungnam National University School of Medicine, Daejeon, Republic of Korea*
[9] *Department of Internal Medicine, Seoul National University College of Medicine, Seoul, Republic of Korea*
[10] *Department of Internal Medicine, Seoul National University Hospital, Seoul, Republic of Korea*
[11] *Cellus Inc., Seoul, Republic of Korea*
[12] *Division of Endocrinology and Metabolism, Department of Internal Medicine, Chungnam National University School of Medicine, Daejeon, Republic of Korea*

**Correspondence to: BS Koo, Department of Otolaryngology-Head and Neck Surgery, Chungnam National University School of Medicine, Daejeon 35015, Republic of Korea. E-mail: bskoo515@cnuh.co.kr; YE Kang, Deparment of Internal Medicine, Chungnam National University School of Medicine, Daejeon 35015, Republic of Korea. E-mail: yeeuni220@cnuh.co.kr*

Abstract

Thyroid cancer is associated with genetic alterations, e.g. $BRAF^{V600E}$, which may cause carcinomatous changes in hormone-secreting epithelial cells. Epidemiological studies have shown that overnutrition is related to the development and progression of cancer. In this study, we attempted to identify the cell nonautonomous factor responsible for the progression of $BRAF^{V600E}$ thyroid cancer under overnutrition conditions. We developed a mouse model for inducible thyrocyte-specific activation of $BRAF^{V600E}$, which showed features similar to those of human papillary thyroid cancer. *LSL-Braf^{V600E};Tg*$CreER^{T2}$ showed thyroid tumour development in the entire thyroid, and the tumour showed more abnormal cellular features with mitochondrial abnormalities in mice fed a high-fat diet (HFD). Transcriptomics revealed that adrenomedullin2 (*Adm2*) was increased in *LSL-Braf^{V600E};Tg*$CreER^{T2}$ mice fed HFD. *ADM2* was upregulated on the addition of a mitochondrial complex I inhibitor or palmitic acid with integrated stress response (ISR) in cancer cells. ADM2 stimulated protein kinase A and extracellular signal-regulated kinase *in vitro*. The knockdown of *ADM2* suppressed the proliferation and migration of thyroid cancer cells. We searched The Cancer Genome Atlas and Genotype-Tissue Expression databases and found that increased *ADM2* expression was associated with ISR and poor overall survival. Consistently, upregulated *ADM2* expression in tumour cells and circulating ADM2 molecules were associated with aggressive clinicopathological parameters, including body mass index, in thyroid cancer patients. Collectively, we identified that ADM2 is released from cancer cells under mitochondrial stress resulting from overnutrition and acts as a secretory factor determining the progressive properties of thyroid cancer.

Keywords: thyroid cancer; obesity; mitokine; ADM2; cancer progression; mitochondria

Received 4 February 2022; Revised 28 July 2022; Accepted 2 August 2022

No conflicts of interest were declared.

Introduction

Excessive nutrients have led to an increase in obesity-related metabolic diseases and are associated with an increased risk and mortality from cancer [1–3]. Obesity is a particularly strong risk factor for colon, renal, pancreatic, endometrial, and breast cancer [4–8]. Previous studies have demonstrated a link between obesity and thyroid cancer [9–12]. Although epidemiological studies have shown that obesity increases the incidence of thyroid cancer, it remains unclear how obesity stimulates the development of or influences the prognosis of this cancer type [13–15].

The obesity–cancer connection mechanisms include anabolic hormonal signalling, systemic inflammation, and

adipocyte-cancer crosstalk [16]. Insulin and insulin-like growth factor levels are increased in obesity and may provide a critical hormonal signal that mediates the proliferation and survival of thyroid cancer [17–20]. Obesity is also associated with chronic systemic inflammation [21]. Tumour necrosis factor-alpha and interleukins (IL-1β, IL-6, and IL-8), the expression of which are also elevated in obesity, are linked to thyroid cancer initiation and progression [22–24]. Recent findings suggest that adipocytes participate in crosstalk with parenchymal cells to promote cancer initiation and progression [25,26]. Robust experimental findings have demonstrated that adipocytes potentiate tumour cell proliferation and invasion in multiple cancers *in vitro* and *in vivo* [26–29]. However, the mechanisms underlying the obesity–thyroid cancer connection remain unclear.

Excess nutrients, including free fatty acids and downstream metabolites such as diacylglycerol and ceramides, directly trigger functional abnormalities in the endoplasmic reticulum (ER) and mitochondria [30,31]. We previously investigated morphological and functional changes in thyroid epithelial cells of obese humans and animal models of diet-induced obesity (DIO), o*b/ob*, and *db/db* mice [32]. Thyroid steatosis and ultrastructural changes, including distension of the ER and mitochondrial distortion in thyroid follicular cells, were uniformly observed in DIO mice and genetically obese *ob/ob* and *db/db* mice. Based on these findings, it is conceivable that uptake of excessive nutrients may lead to altered cellular metabolism in thyroid cancer cells and change the tumour properties via cell-autonomous and noncell-autonomous mechanisms.

The mitokine adrenomedullin2 (ADM2) is a cytokine secreted by metabolic stresses (ER stress, mitochondria stress, and integrated stress response). ADM2 belongs to the CGRP/calcitonin family and is involved in cardiovascular homeostasis, food intake regulation, and immune regulation through the calcitonin receptor-like/calcitonin receptor-like receptor (CALCRL/RAMP) complex [33–36]. ADM2 expression is induced by bacterial lipopolysaccharide, thyroid-stimulating hormone, oestrogen exposure, mitochondrial dysfunction, hypoxia, and obesity [37–41]. ADM2 is considered a prognostic marker or therapeutic target in pancreatic adenocarcinoma, breast cancer, and hepatocellular carcinoma [42–44], but its role in thyroid cancer remains unclear.

To address whether excessive nutrients directly affect thyroid tumour behaviour *in vivo*, we utilised the thyrocyte-specific $BRAF^{V600E}$ mutation, the most frequently occurring mutation in human thyroid cancer, in a mouse model, which was constructed at the adult stage [45]. This study shows that tumours featured more aggressive cellular characteristics and ultrastructural mitochondrial abnormalities in response to a high-fat diet (HFD).

Materials and methods

Animal experiments

Animals received humane care, and protocols were approved by the Institutional Animal Care and Use Committee of Chungnam National University School of Medicine (Daejeon, Republic of Korea).

To generate thyrocyte-specific $BRAF^{V600E}$ knock-in mice, lox-stop-lox (*LSL*)-$Braf^{V600E}$ mice (a kind gift from James A Fagin, Memorial Sloan Kettering Cancer Center, New York, NY, USA) were crossed with *thyroglobulin*-$CreER^{T2}$ ($TgCreER^{T2}$) mice (a kind gift from Jukka Kero, University of Turku, Åbo FI-20521, Finland) on a C57BL/6 background [46,47]. Mice were acclimated to a 12-h light/12-h dark cycle, temperature (23 °C), and 50–60% humidity environment and fed a chow diet (CD). Tamoxifen (Sigma-Aldrich, St. Louis, MO, USA) was administered at a total dose of 5 mg for 5 days. The mouse model of DIO was developed by feeding HFD (60% of total energy intake as fat, TD.06414, ENVIGO, Indianapolis, IN, USA). Tissues were obtained when mice were euthanized. All mice used in this study were male.

RNA sequencing

Total RNA was isolated using TRIzol reagent (Life Technologies, Eugene, OR, USA) and transcribed into complementary DNA (cDNA) following the TruSeq Stranded Total RNA Sample Prep Guide (Illumina, San Diego, CA, USA). Low-quality sequence artefacts were removed. Reads were mapped to the reference genome (*Mus musculus*, mm10) using HISAT2 or Kalisto. Differential expression analysis (DEA) was performed using the R (R Foundation, Vienna, Austria) package DEseq2. Transcript abundance was transformed into fragments per kilobase of transcript per million after transcript quantification. Gene set enrichment analysis (GSEA) was conducted with PIANO within the R program using gene sets obtained from Enrichr (https://maayanlab.cloud/Enrichr/).

Transmission electron microscopy

Thyroid tissues were fixed with 1% glutaraldehyde at 4 °C and washed with 0.1 M cacodylate buffer. Tissues were fixed for 1 h at 4 °C with 1% OsO_4 in 0.1 M cacodylate buffer, pH 7.2, containing 0.1% $CaCl_2$. They were then embedded in Embed-812 (Electron Microscopy Sciences, Hatfield, PA, USA) and polymerized at 60 °C for 36 h. Embedded samples were sectioned using an EM UC6 ultramicrotome (Leica Biosystems, Heidelberger str, Nußloch, Germany) and stained with 4% (w/v) uranyl acetate and lead citrate. Stained samples were examined using a Leo912 transmission electron microscope (Carl Zeiss, Oberkochen, Germamy) at 120 kV.

In vitro cell culture

BCPAP and 8505c (DSMZ, Braunschweig, Germany) cells were cultured in RPMI 1640 medium (Welgene, Daejeon, Republic of Korea) supplemented with 10% foetal bovine serum (FBS; Gibco, Waltham, MA, USA), 100 U/ml penicillin, and 100 µg/ml streptomycin at 37 °C in a humidified atmosphere with 5% CO_2. Rotenone (Sigma-Aldrich) was diluted with ethanol. Palmitate was conjugated with bovine serum albumin (BSA) according to the protocol of Seahorse Bioscience (North Billerica, MA,

USA). Cell lines were treated with 1 μM rotenone or 50 μM BSA-conjugated palmitic acid for 24 h. ADM2 recombinant protein (MyBioSource, San Diego, CA, USA) was added to cell lines for 12 h. The genetic disruption of *ADM2* was performed using human shRNA lentiviral particles (sh*ADM2*; TL306813V) from OriGene Technologies (Rockville, MD, USA). Scrambled shRNA lentiviral particles (shCtrl; TR30021V; OriGene Technologies) were used as controls.

Oxygen consumption rate analysis

Cells were plated at a concentration of 1×10^4 per well on Seahorse XF-24 plates (Seahorse Bioscience) overnight. BSA-conjugated palmitic acid was added for 24 h after the cells had attached to the wells. A calibration cartridge (#102416-100, Seahorse Bioscience) was activated overnight in a non-CO_2-containing incubator. On the measurement day, the cell medium was changed to XF assay medium (#102365-100, Seahorse Bioscience), and cells were incubated in a non-CO_2-containing incubator for 1 h. The XF-24 analyser was calibrated using the calibration cartridge. After calibration, the cell plate was loaded onto Seahorse XF-24 extracellular flux analyser (Seahorse Bioscience), and mitochondrial function was measured with inhibitors: oligomycin (2 μg/ml), carbonyl cyanide 3-chlorophenylhydrazone (10 μM), and rotenone (1 μM).

Analysis of the Genotype-Tissue Expression (GTEx) and the Cancer Genome Atlas (TCGA) dataset

Survival analyses were performed using GEPIA2 (http://gepia2.cancer-pku.cn/). Expression levels of *ADM2* and

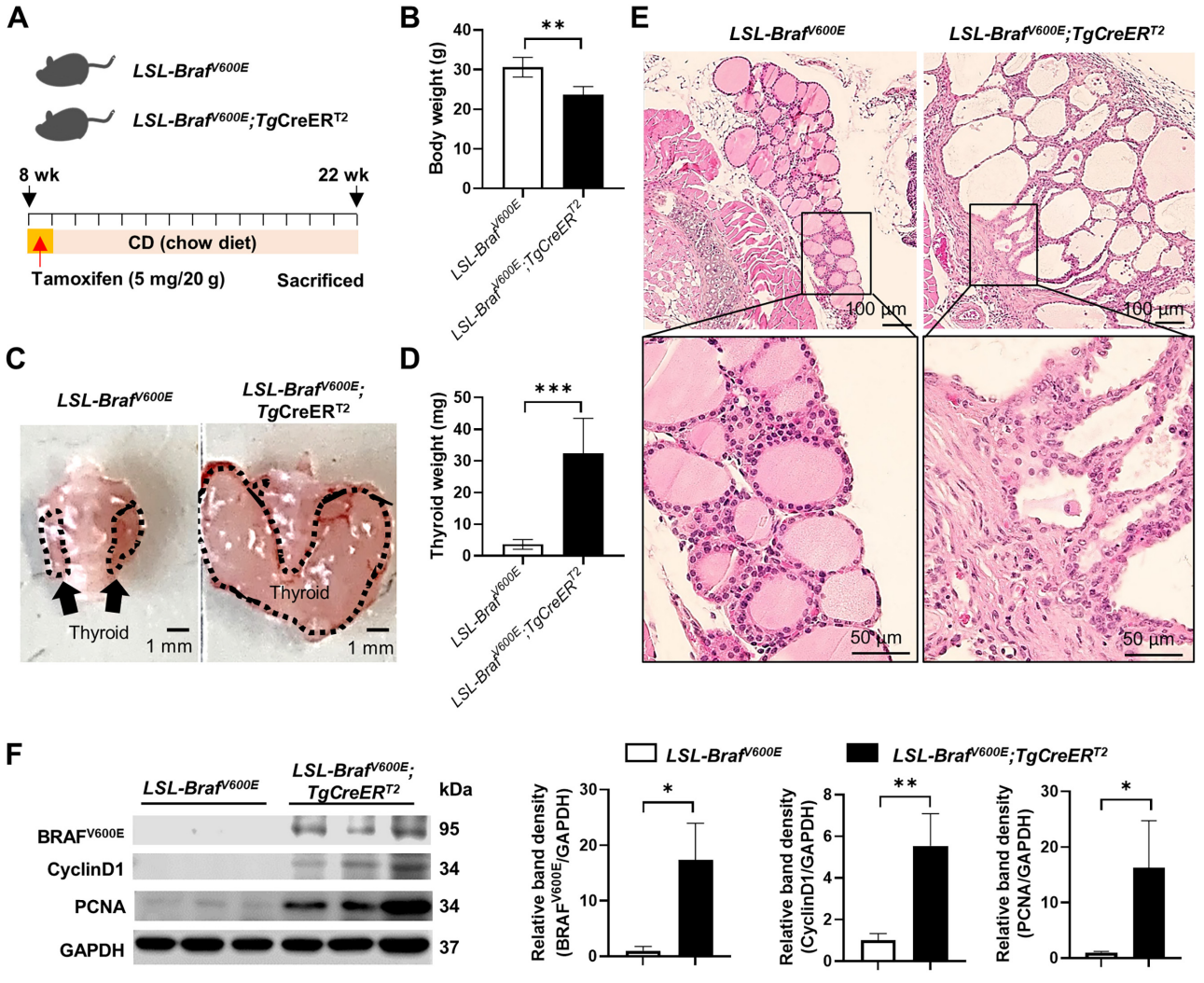

Figure 1. *LSL-Braf*^{V600E};*Tg*CreER^{T2} mice developed a solid mass region with papillary growing with dysmorphic and variable follicles on administration of tamoxifen. (A) Diagram of the experimental design. Tamoxifen was injected into *LSL-Braf*^{V600E} mice and *LSL-Braf*^{V600E};*Tg*CreER^{T2} mice at 8 weeks of age to induce Braf^{V600E} knock-in. All mice were sacrificed at 22 weeks of age. (B) Body weight of *LSL-Braf*^{V600E} mice and *LSL-Braf*^{V600E};*Tg*CreER^{T2} mice at 22 weeks of age (*LSL-Braf*^{V600E} mice, $n = 8$; *LSL-Braf*^{V600E};*Tg*CreER^{T2}, $n = 3$). (C) Representative gross image of thyroid glands in *LSL-Braf*^{V600E} mice and *LSL-Braf*^{V600E};*Tg*CreER^{T2} mice. (D) Thyroid weight of *LSL-Braf*^{V600E} mice and *LSL-Braf*^{V600E};*Tg*CreER^{T2} mice (*LSL-Braf*^{V600E} mice, $n = 7$; *LSL-Braf*^{V600E};*Tg*CreER^{T2}, $n = 3$). (E) Histological images of the thyroid gland in *LSL-Braf*^{V600E} mice and *LSL-Braf*^{V600E}; *Tg*CreER^{T2} mice. (F) Immunoblot analysis of BRAF^{V600E}, CyclinD1, PCNA, and GAPDH in thyroid gland from *LSL-Braf*^{V600E} mice and *LSL-Braf*^{V600E};*Tg*CreER^{T2} mice (*LSL-Braf*^{V600E} mice, $n = 8$; *LSL-Braf*^{V600E};*Tg*CreER^{T2}, $n = 3$). Mean ± SEM. *$p < 0.05$ or **$p < 0.01$ or ***$p < 0.001$ (two-tailed Student's *t*-test).

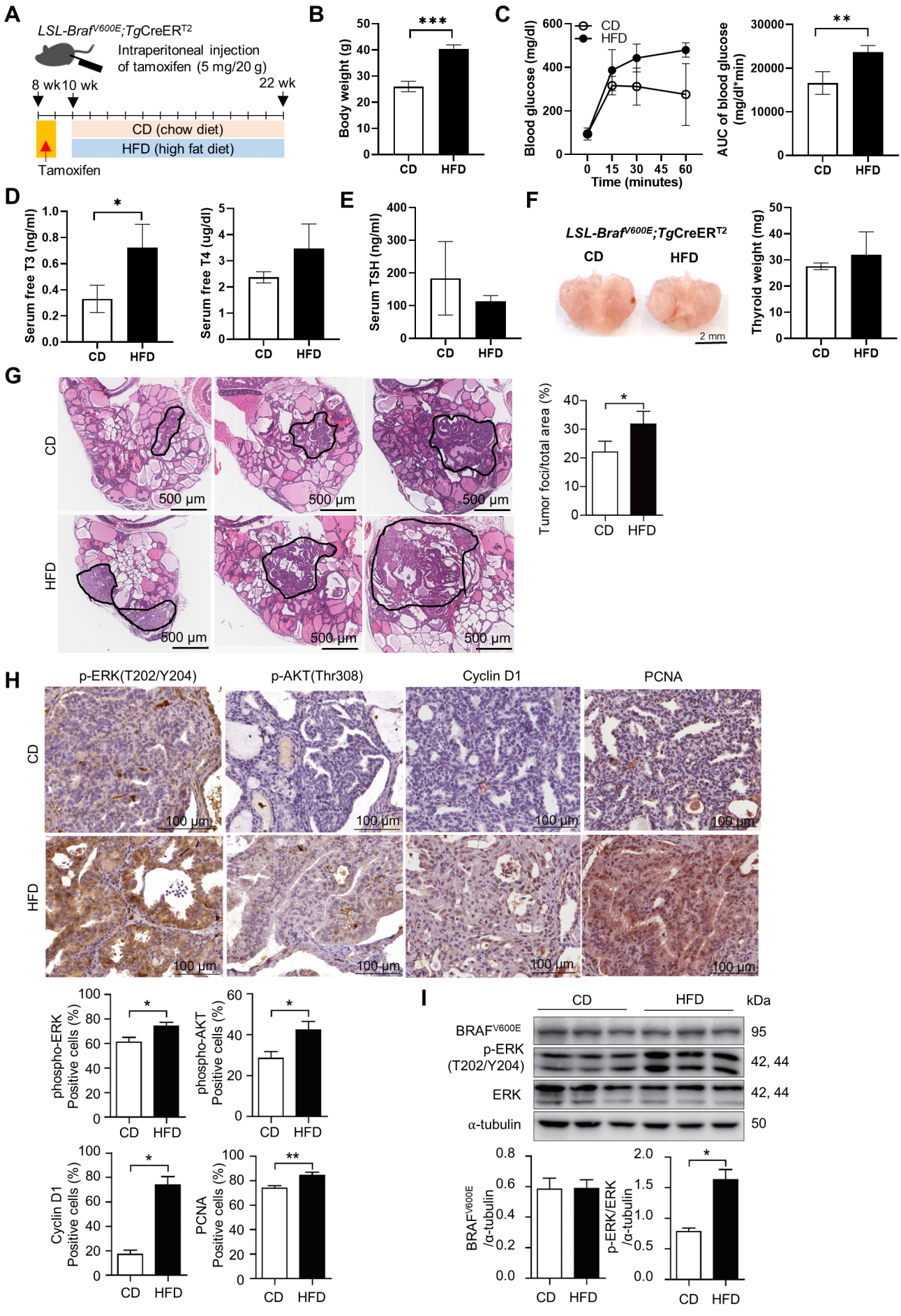

Figure 2 Legend on next page.

RAMPs were downloaded from the GTEx portal (http://gtexportal.org/). The TCGA-THCA dataset was obtained from the UCSC database (http://xena.ucse.edu/). To elucidate the role of ADM2, we divided THCA into two groups based on *ADM2* expression by quartile. DEA and GSEA were performed using DESeq2 and PIANO [48,49].

Statistical analyses

The data shown represent at least three independent experiments. The *in vivo* data were replicated using individual mice. Data are expressed as mean ± standard error (SEM). Statistical analyses were performed using GraphPad Prism 9 (GraphPad Software, San Diego, CA, USA). Data were analysed using one-way analysis of variance (more than two groups), Student's two-tailed *t*-test (two groups), or univariate analysis using stepwise logistic regression.

Results

Characteristics of the thyrocyte-specific *Braf*^{V600E}-inducible mice

We developed a mouse model for inducing thyrocyte-specific *BRAF*^{V600E} mutations by crossing *LSL-Braf*^{V600E} and *Tg*CreER^{T2} mice to generate *LSL-Braf*^{V600E};*Tg*CreER^{T2} mice. Tamoxifen was administered at 8 weeks of age to induce expression of BRAF^{V600E}, and the mice were sacrificed at 22 weeks of age (Figure 1A). The body weight of *LSL-Braf*^{V600E};*Tg*CreER^{T2} mice was lower than that of the *LSL-Braf*^{V600E} mice (Figure 1B). *LSL-Braf*^{V600E};*Tg*CreER^{T2} mice developed goitres (Figure 1C). *LSL-Braf*^{V600E};*Tg*CreER^{T2} mice had significantly increased thyroid weight compared to *LSL-Braf*^{V600E} mice (Figure 1D). The thyroids of *LSL-Braf*^{V600E};*Tg*CreER^{T2} mice had dysmorphic and variable follicles and formed a solid mass region with papillary growth (Figure 1E). The levels of Braf^{V600E} and proliferation-related proteins (CyclinD1 and PCNA) were significantly increased in *LSL-Braf*^{V600E};*Tg*CreER^{T2} mice compared to *LSL-Braf*^{V600E} mice (Figure 1F).

Impact of an HFD on thyrocyte-specific Braf^{V600E}-inducible mice

To investigate the effect of obesity on thyroid cancer behaviour, *LSL-Braf*^{V600E};*Tg*CreER^{T2} mice were put on an HFD after tamoxifen administration (Figure 2A). *LSL-Braf*^{V600E};*Tg*CreER^{T2} mice fed HFD for 12 weeks showed increased body weight, white adipose tissue, and liver weight compared to CD-fed mice (Figure 2B and supplementary material, Figure S1A) and developed systemic glucose tolerance (Figure 2C). Moreover, plasma levels of alanine aminotransferase (ALT) and total cholesterol increased in HFD-fed mice (supplementary material, Figure S1B,C). Serum-free T3 increased in HFD-fed compared with that in CD-fed mice. There was no change in serum-free T4 and thyroid stimulating hormone (TSH) concentration (Figure 2D,E). HFD-fed mice showed an increased percentage of tumour foci/total thyroid area, although there was no difference in thyroid weight (Figure 2F,G). Furthermore, HFD-fed mice had an increased proportion of nuclear clearing cells and oncocytic-changed cells, which is related to the accumulation of abnormal mitochondria (supplementary material, Figure S1D,E). Increased phospho-ERK (T202/Y204), phospho-AKT (Thr308), Cyclin D1, and PCNA levels were observed in HFD-fed mice (Figure 2H); however, the expression of BRAF^{V600E} was similar in the two groups (Figure 2I). Additionally, western blotting analysis of the entire thyroid gland including nontumour foci, showed increased p-AKT and an increasing trend for PCNA and CyclinD1 in HFD-fed mice (supplementary material, Figure S1G). The expression of immune cell markers (CD4, CD8, and CD163) was not detected in the tumour region in LSL-*Braf*^{V600E};*Tg*CreER^{T2} mice fed with either CD or HFD (supplementary material, Figure S2). Lymphovascular invasion and extrathyroid extension were absent in both groups (data not shown). Our results show that HFD activated thyroid tumour proliferation through additional factors via the extracellular signal-regulated kinase (ERK) signalling pathway.

Induction of ADM2 by metabolic stress

To identify the factors related to the progressive features of thyroid tumours in HFD-fed LSL-*Braf*^{V600E};*Tg*CreER^{T2} mice, we analysed transcriptomes. Among the 20 genes that showed significantly altered expression (adjusted

Figure 2. Diet-induced obesity causes tumour progression in *LSL-Braf*^{V600E};*Tg*CreER^{T2} mice. (A) Diagram of the experimental design. Tamoxifen was injected at 8 weeks of age. CD and HFD were fed for 12 weeks starting at 10 weeks of age. All mice were sacrificed at 22 weeks of age. (B) Body weight of *LSL-Braf*^{V600E};*Tg*CreER^{T2} mice fed CD or HFD at 22 weeks of age (*LSL-Braf*^{V600E};*Tg*CreER^{T2} mice fed CD, $n = 3$; *SL-Braf*^{V600E};*Tg*CreER^{T2} mice fed HFD, $n = 5$). (C) Glucose tolerance test at 20 weeks of age. Glucose (1 g/kg) was administered, and blood glucose was measured at 0, 15, 30, 45, and 60 min ($n = 4$). (D) Serum concentration of thyroid hormones (free T3 and free T4) (*LSL-Braf*^{V600E};*Tg*CreER^{T2} mice fed CD, $n = 3$; *SL-Braf*^{V600E};*Tg*CreER^{T2} mice fed HFD, $n = 5$). (E) Serum concentration of TSH (*LSL-Braf*^{V600E};*Tg*CreER^{T2} mice fed CD, $n = 3$; *SL-Braf*^{V600E};*Tg*CreER^{T2} mice fed HFD, $n = 4$). (F) Thyroid images and weight of *LSL-Braf*^{V600E};*Tg*CreER^{T2} mice fed CD or HFD at 22 weeks of age (*LSL-Braf*^{V600E};*Tg*CreER^{T2} mice fed CD, $n = 3$; *SL-Braf*^{V600E};*Tg*CreER^{T2} mice fed HFD, $n = 5$). (G) Most enlarged region of cancer foci and tumour foci/total area, black lines indicate tumour foci ($n = 4$). (H) Immunohistochemistry images and graph on thyroid cancer tissue ($n = 4$). (I) Immunoblot analysis of BRAF^{V600E}, CyclinD1, p-ERK, ERK, and α-tubulin of the thyroid gland from *LSL-Braf*^{V600E};*Tg*CreER^{T2} mice fed CD or HFD ($n = 3$). Mean ± SEM. *$p < 0.05$ or **$p < 0.01$ or ***$p < 0.001$ (two-tailed Student's *t*-test).

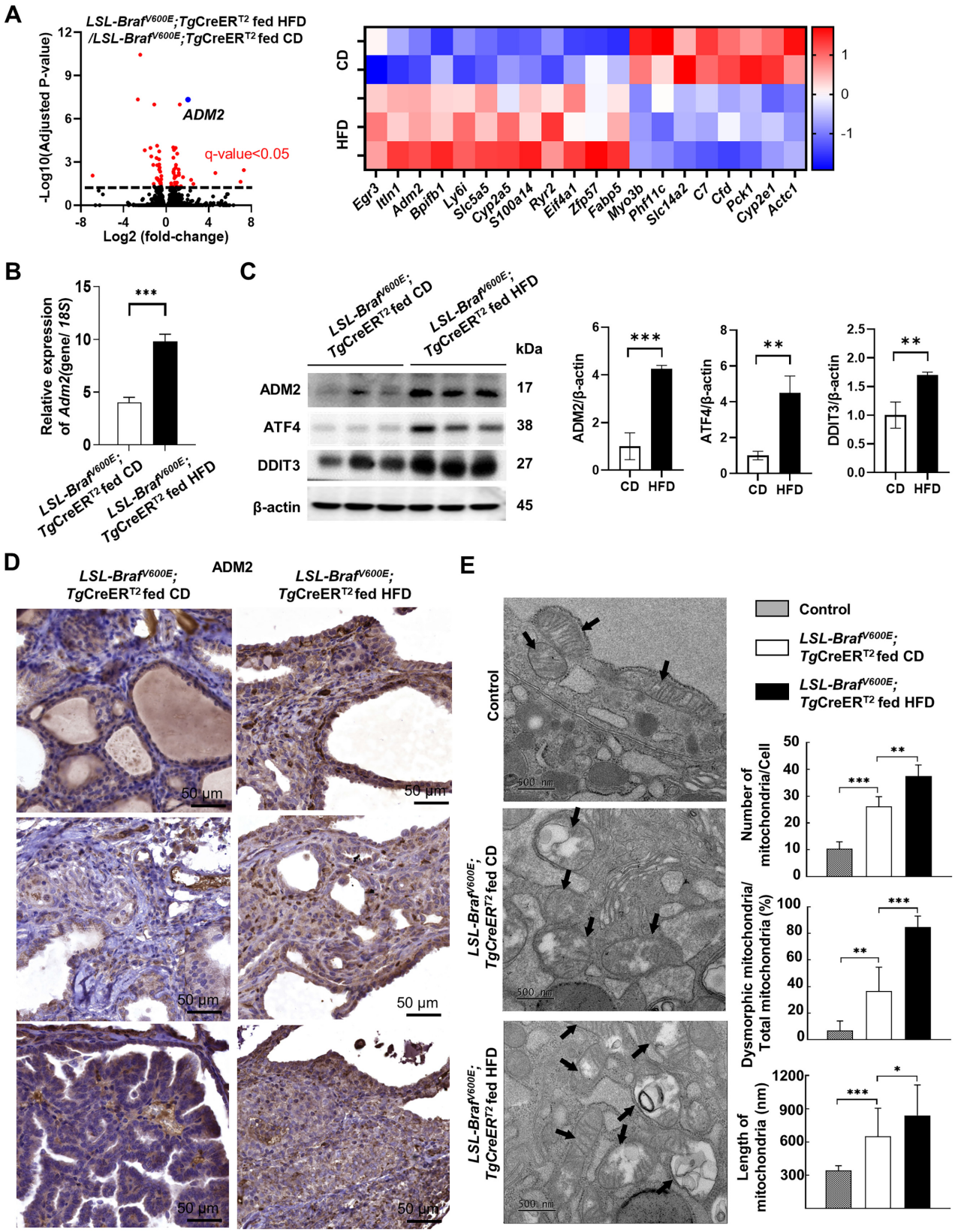

Figure 3. Transcriptome analyses revealed that ADM2 is upregulated by metabolic stress in the thyroid gland of *LSL-Braf*$^{V600E;}$*Tg*CreER^{T2} mice. (A) Volcano plot and heat map of RNA*seq* analysis from *LSL-Braf*$^{V600E;}$ *Tg*CreER^{T2} mice fed CD or HFD (*LSL-Braf*^{V600E};*Tg*CreER^{T2} mice fed CD, $n = 2$; *SL-Braf*^{V600E};*Tg*CreER^{T2} mice fed HFD, $n = 3$). (B) RT-qPCR analysis of *Adm2* mRNA expression in thyroid gland from *LSL-Braf*^{V600E}; *Tg*CreER^{T2} mice fed CD or HFD ($n = 5$). (C) Immunoblot analysis of ADM2, ATF4, DDIT3, and β-actin of the thyroid gland from *LSL-Braf*^{V600E};*Tg*CreER^{T2} mice fed CD or HFD ($n = 3$). (D) Representative immunohistochemistry images of ADM2 expression in thyroid gland from *LSL-Braf*$^{V600E;}$*Tg*CreER^{T2} mice fed CD or HFD; scale bars: 50 μm ($n = 4$). (E) Electron microscopy analysis of thyrocytes from *LSL-Braf*$^{V600E;}$*Tg*CreER^{T2} mice, black arrows indicate mitochondria; scale bars, 500 nm ($n = 5$). Mean ± SEM. $^{*}p < 0.05$ or $^{**}p < 0.01$ or $^{***}p < 0.001$ (two-tailed Student's *t*-test).

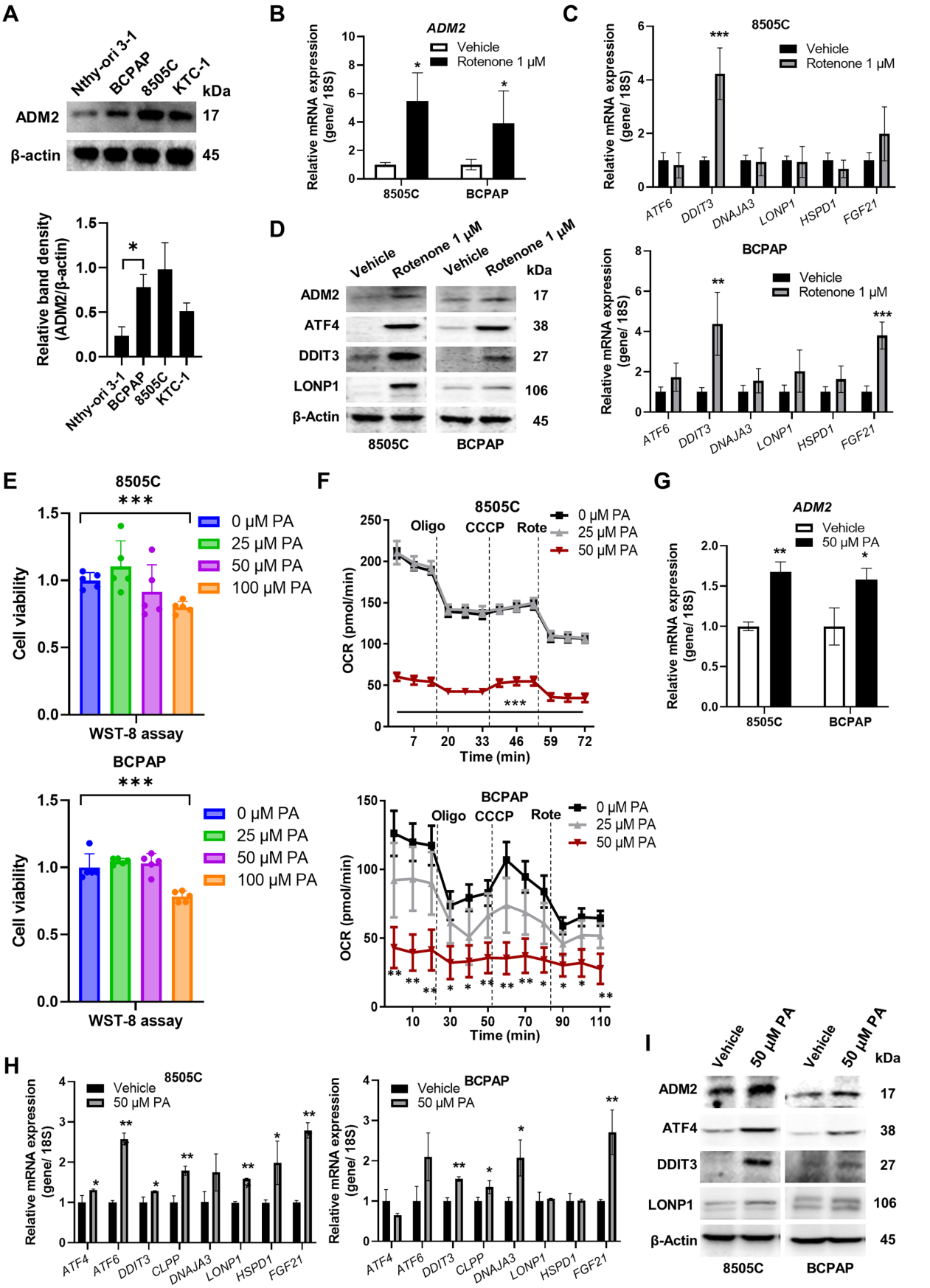

Figure 4 Legend on next page.

$p < 0.05$), *Adm2* was the most significantly increased gene in mice on HFD compared to CD (Figure 3A). The expression of *Adm2* was upregulated approximately two-fold in *LSL-Braf*^{V600E};*Tg*CreER^{T2} mice fed HFD compared to those fed CD according to RT-qPCR (Figure 3B). Additionally, HFD-fed mice had increased expressions of ADM2 and integrated stress response (ISR)-related proteins (ATF4 and DDIT3) (Figure 3C). Immunohistochemistry showed that although tumour cells expressed ADM2 in LSL-*Braf*^{V600E};*Tg*CreER^{T2} mice fed CD, HFD-fed mice had a larger population of ADM2-positive cells and increased expression of ADM2 in tumour cells (Figure 3D). HFD-fed *LSL-Braf*^{V600E} mice exhibited increased ADM2 and reduced phospho-ERK expression compared to CD-fed *LSL-Braf*^{V600E} mice, although no differences were observed in thyroid size between the groups (supplementary material, Figure S3). We observed increased cells with an oncocytic change in *LSL-Braf*^{V600E};*Tg*CreER^{T2} mice fed an HFD (supplementary material, Figure S1E). In addition, we found that thyrocytes of HFD-fed mice had dysmorphic mitochondria, which were swollen and had collapsed cristae and an increased number of mitochondria than CD-fed mice (Figure 3E). Collectively, our findings indicate that HFD induced ADM2 expression in thyrocytes with dysmorphic mitochondria in *LSL-Braf*^{V600E};*Tg*CreER^{T2} mice.

Upregulation of ADM2 by mitochondrial complex I inhibitor or palmitic acid treatment

Compared with the immortalised thyroid cell line (Nthy-ori 3-1) the BRAF mutated cancer cell lines (BCPAP, 8505C, KTC-1) had increased expression of ADM2 (Figure 4A). The expression of ADM2 was analysed in BCPAP, a papillary thyroid cancer (PTC) cell line, and 8505C, an anaplastic thyroid cancer cell line, which originated from a primary region of cancer. We examined whether the expression of ADM2 was regulated by metabolic stress, particularly the mitochondrial stress response. Treatment with rotenone, an inhibitor of OxPhos complex I, led to a significant increase in *ADM2* expression in 8505C and BCPAP cells (Figure 4B). In addition, rotenone induced increased expression of the ISR-related genes *DDIT3* in both cancer lines and *FGF21*, in BCPAP cells (Figure 4C), and protein expressions of ADM2, ATF4, DDIT3, and LONP1 were upregulated by rotenone (Figure 4D).

Next, we examined mitochondrial function and ADM2 expression after fatty acid treatment. Palmitic acid, the most common saturated fatty acid, is increased in obesity and induces intracellular metabolic stress [50]. We performed an oxygen consumption rate analysis to measure mitochondrial function in thyroid cancer cells treated with palmitic acid. There was no difference in viability up to 50 μM palmitic acid, but viability decreased at 100 μM (Figure 4E). Cancer cell lines treated with 50 μM palmitic acid reduced their oxygen respiration rates compared with vehicle controls (Figure 4F). Palmitic acid stimulated the expression of *ADM2* in thyroid cancer cell lines (Figure 4G) and induced the expression of *ATF4*, *ATF6*, *DDIT3*, *CLPP*, *LONP1*, *HSPD1*, and *FGF21* in 8505C cells and *DDIT3*, *CLPP*, *DNAJA3*, and *FGF21* in BCPAP cells (Figure 4H). The expression of the proteins ADM2, ATF4, DDIT3, and LONP1 also increased (Figure 4I). Collectively, these results suggest that metabolic stress stimulates ADM2 expression along with induction of the ISR in thyroid cancer cell lines.

Cell proliferation and migration by ADM2 via ERK signalling *in vitro*

To ascertain whether ADM2 accelerates cancer progression, we analysed the effects of recombinant ADM2 treatment or sh*ADM2* in a cancer cell line. First, we confirmed that ERK was phosphorylated by recombinant ADM2. Treating cells with 20 nM of recombinant ADM2 resulted in the phosphorylation of PKA substrates and ERK (T202/Y204) in the thyroid cancer cell lines (Figure 5A). Knockdown of *ADM2* was performed. Transfection with sh*Adm2* reduced the expression of ADM2 in cancer cell lines (Figure 5D). The sh*ADM2*-transfected cell lines showed reduced proliferation and migration than the shCtrl-transfected cell line (Figure 5B,C). Moreover, *shADM2*-transfected cells showed decreased phosphorylation of ERK (T202/Y204), AKT (Thr308), STAT3 (Ser727), and NF-κB (Ser536) compared to shCtrl-transfected cells (Figure 5D). These results demonstrate that ADM2 promotes thyroid cancer progression by stimulating the phosphorylation of ERK signalling.

Association of ADM2 with the ISR pathway and poor survival rates in thyroid cancer in humans

To elucidate the role of ADM2 in human subjects, we investigated RNA*seq* data from the human databases

Figure 4. Metabolic stress induces the expression of *ADM2* and the activation of ISR signalling pathways in the thyroid cancer cell line. (A) ADM2 expression in thyroid cell lines. (B) RT-qPCR analysis for *ADM2* mRNA in thyroid cancer cell lines in the presence or absence of rotenone (1 μM) for 24 h ($n = 3$). (C) RT-qPCR analysis for ISR and mitokine genes of thyroid cancer cell lines in the presence or absence of rotenone (1 μM) ($n = 3$). (D) Immunoblot analysis of ADM2 and ISR-related proteins of thyroid cancer cell line in the presence or absence of rotenone (1 μM). (E) Cell viability test using a wst-8 assay of a thyroid cancer cell line after 24 h treatment of palmitic acid (0, 25, 50, 100 μM) ($n = 5$). (F) Oxygen consumption rates (OCR) of thyroid cancer cell lines after 24 h treatment with palmitic acid (0, 25, and 50 μM) (8505C, $n = 4$; BCPAP, $n = 5$). CCCP: carbonyl cyanide m-chlorophenyl hydrazone. (G) RT-qPCR analysis for *ADM2* mRNA in thyroid cancer cell lines treated with 50 μM palmitic acid for 24 h ($n = 3$). (H) RT-qPCR analysis for ISR and mitokine genes in a thyroid cancer cell line treated with 50 μM palmitic acid for 24 h ($n = 3$). (I) Immunoblot analysis for ADM2 and ISR-related proteins from thyroid cancer cell lines treated with 50 μM palmitic acid for 24 h. Mean ± SEM. *$p < 0.05$ or **$p < 0.01$ or ***$p < 0.001$ (two-tailed Student's *t*-test).

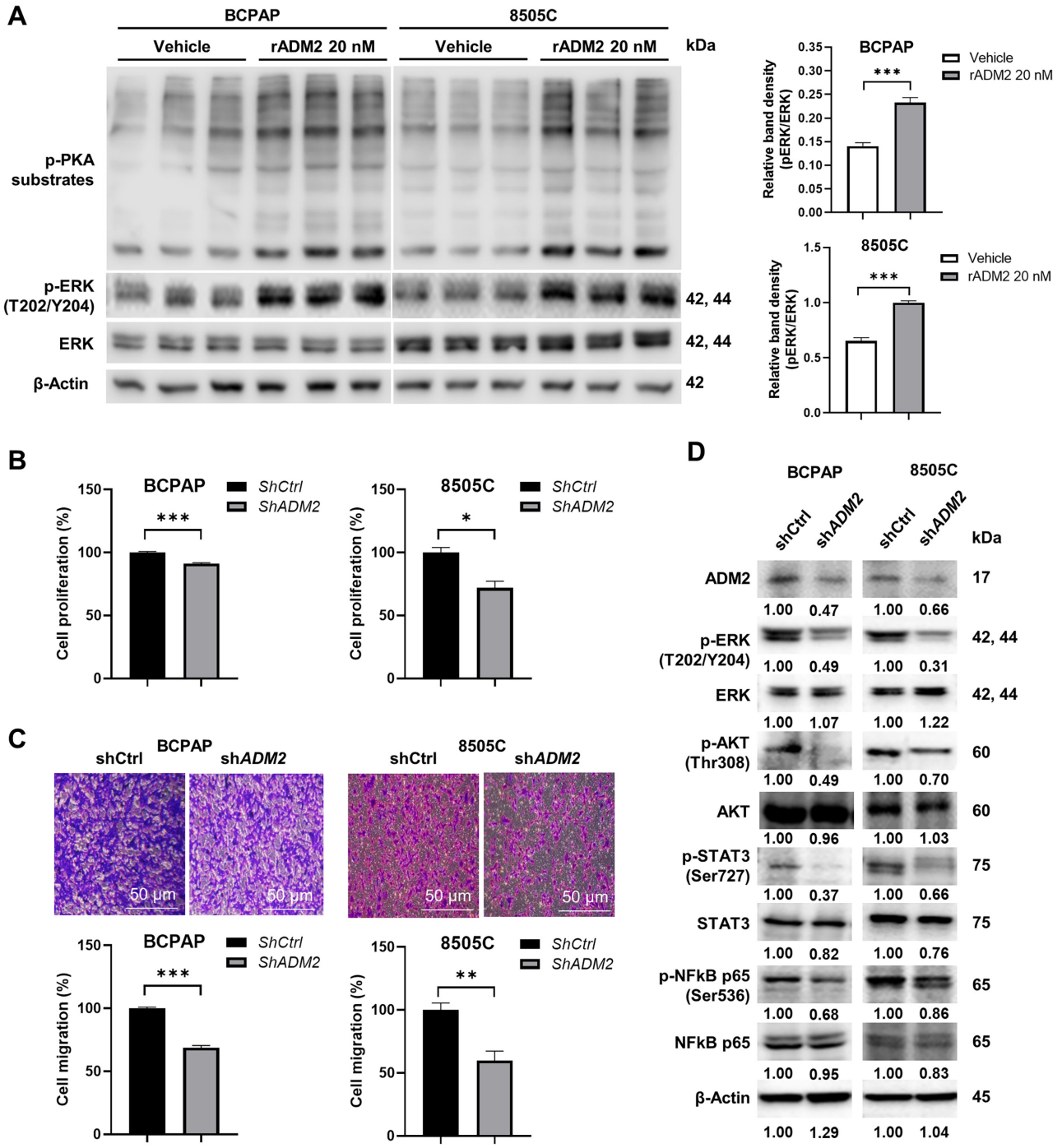

Figure 5. ADM2 deficiency slows cell proliferation and migration of thyroid cancer cell lines through ERK signalling. (A) Immunoblot analysis of recombinant AMD2-induced PKA and ERK signal ($n = 3$). (B) Proliferation analysis in the thyroid cancer cell line transfected with sh*ADM2* ($n = 3$). (C) Migration analysis in the thyroid cancer cell line transfected with sh*ADM2* ($n = 3$). (D) Immunoblot analysis for ADM2, AKT, ERK, STAT3, and NF-*k*B in the thyroid cancer cell lines transfected with sh*ADM2*. Mean ± SEM. *$p < 0.05$ or **$p < 0.01$ or ***$p < 0.001$ (two-tailed Student's *t*-test).

GTEx (a public database providing nondisease tissue for molecular assays, including RNA*seq*) and TCGA (a landmark genomics program for cancer providing molecular characteristics). We compared *ADM2* expression between organs. The expression of *ADM2* in the thyroid gland was 19.1, while the mean expression of *ADM2*, excluding the thyroid gland, was 1.15. The kidney had the second-highest expression value, which was 5.8 (supplementary material, Figure S4A). Using correlation analysis, we examined whether the expression of *ADM2* was associated with metabolic stress genes. Expression of the ISR genes (*DDIT3*, *ATF4*, and *LONP1*) was significantly correlated with *ADM2* expression in the normal thyroid gland (Figure 6A) and the thyroid cancer dataset (Figure 6B). However, expression of *ADM2* and *ATF4* was reduced in tumour tissues (supplementary material, Figure S4B), although *LONP1* expression increased (supplementary material, Figure S4B). These data suggested

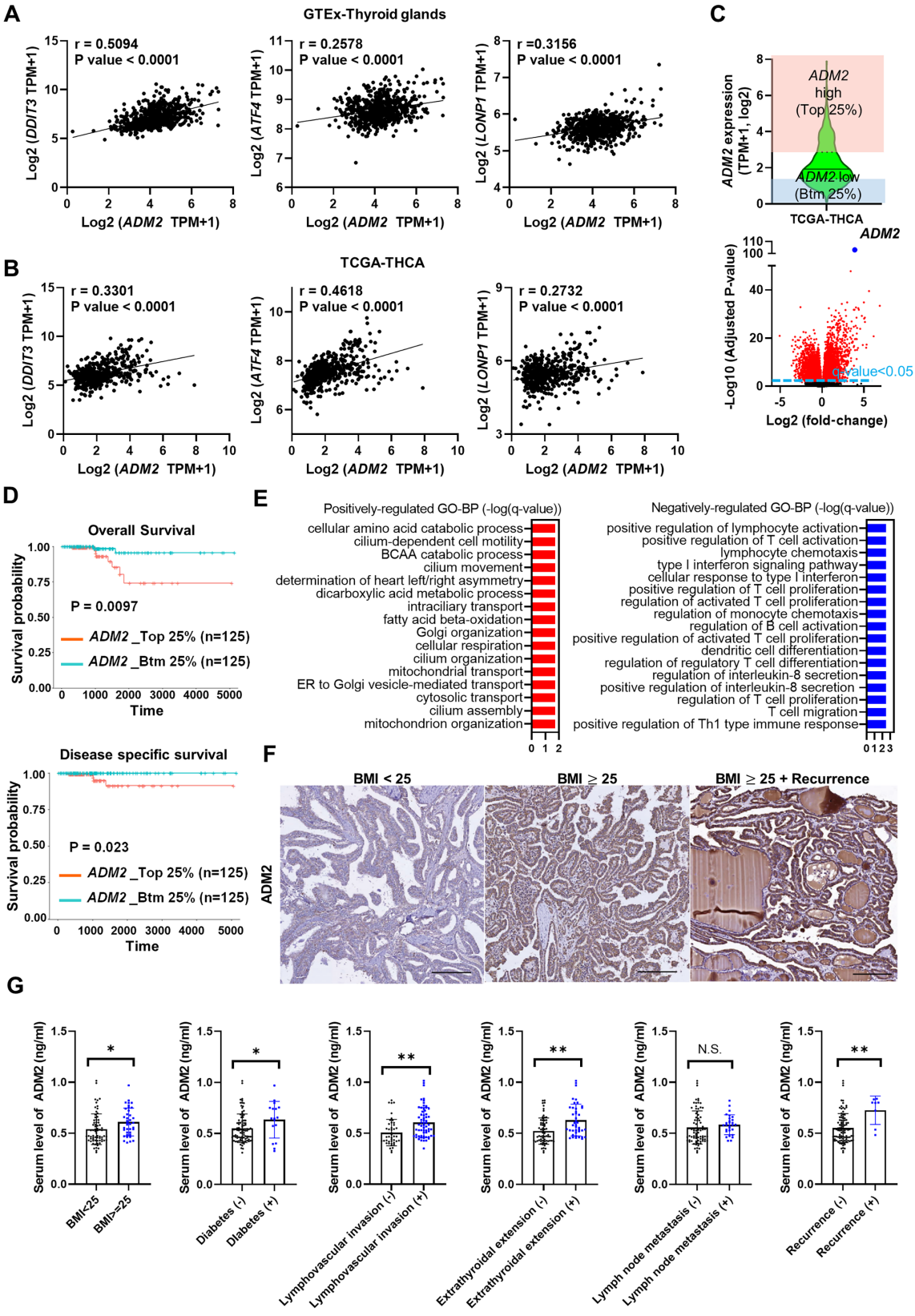

Figure 6. ADM2 is related to the ISR and poor clinicopathological features in human thyroid. (A and B) Correlation analysis of ADM2 with ISR genes (A) GTEx-Thyroid gland. (B) TCGA-THCA. (C–E) Comparison of groups divided using *ADM2* expression on quartile in TCGA-THCA. (C) The violin and volcano plots. (D) Overall survival and disease-specific survival. (E) Bar plots representing the gene set enrichment analysis of Gene-Ontology biological process. (F) Comparisons in CNUH cohort and (G) Immunoblot analysis for ADM2 in the thyroid gland of PTC patients. Serum level of ADM2 in PTC patients divided by clinicopathological features. Mean ± SEM. *$p < 0.05$ or **$p < 0.01$.

the distinct role of ADM2 and ISR in normal and tumour tissues. To predict the role of *ADM2* in tumour aggressiveness, patients with thyroid cancer were classified according to *ADM2* expression levels into a top (high *ADM2* expression) and bottom 25% group (low *ADM2* expression) (Figure 6C). Interestingly, the top 25% group

Table 1. Logistic regression analysis of the relationship between ADM2 staining and clinicopathological factors

Factors	Exp(β)	SE	95% CI	*P* value
Body mass index	1.236	0.072	(1.074, 1.424)	0.003*
Tumour size	1.802	0.272	(1.058, 3.069)	0.030*
Lymph node metastasis	2.330	0.656	(1.147, 4.733)	0.019*
Recurrence	1.685	0.656	(0.466, 6.095)	0.173

CI, confidence interval; Exp(β), odds ratio; SE, standard error.
*Statistically significant.

showed lower overall and disease-specific survival than that of the bottom 25% group (log-rank $p = 0.043$) (Figure 6D). The same trend was found in the non-BRAF and BRAF subtypes (supplementary material, Figure S5A), although it was not significant. There was no difference in survival between the groups classified by ADM2 receptors (*RAMP1*, *RAMP2*, and *RAMP3*) (supplementary material, Figure S5B). We identified the pathways related to *ADM2* using gene ontology analysis. Interestingly, fatty acid beta-oxidation, mitochondrial transport, and mitochondrial organization were upregulated in the top 25% group. Furthermore, we observed that differentially expressed genes were associated with fatty acid degradation, the tricarboxylic acid cycle, and oxidative phosphorylation pathways in the Kyoto Encyclopedia of Genes and Genomes (KEGG) (Figure 6E and supplementary material, Figure S6). By contrast, immune-related processes were enriched in the group with low *ADM2* expression (Figure 6E). Collectively, these results suggest that *ADM2* is potentially an oncogenic factor *in silico* as well as *in vivo* and *in vitro*.

Association of ADM2 with aggressive clinicopathologic parameters and obesity in thyroid cancer

To evaluate the relationship between obesity-induced ADM2 expression and tumour aggressiveness, we investigated the clinicopathologic features, including body mass index (BMI), associated with samples from 160 PTC patients treated at Chungnam National University Hospital (CNUH) from 2003 to 2010. Patients were divided into two groups according to ADM2 immunoreactivity (supplementary material, Table S1). High ADM2 expression was significantly associated with clinicopathological parameters, including BMI, tumour size, lymph node metastasis, and locoregional recurrence. To assess the usefulness of ADM2 expression as an independent predictor of aggressive PTC phenotypes, multivariate analysis using stepwise logistic regression was conducted (Table 1). This showed that high ADM2 expression was an independent risk factor for BMI ($p = 0.003$, odds ratio [OR] 1.236), tumour size ($p = 0.030$, OR 1.802), and the presence of lymph node (LN) metastasis ($p = 0.019$, OR 2.330). Thus, ADM2 expression was highly associated with obesity and tumour recurrence (Figure 6F and supplementary material, Figure S7).

Patients were divided into two groups according to their ADM2 serum levels (supplementary material, Table S2). The high circulating ADM2 group showed increased BMI and fasting glucose levels. Moreover, circulating ADM2 levels were significantly associated with the presence of extrathyroidal extension, lymphovascular invasion, and lymph node metastasis. The ADM2 levels were significantly higher in obese patients (BMI ≥ 25) than in lean patients (BMI < 25). Patients with diabetes showed increased ADM2 levels compared to nondiabetic patients. Furthermore, the mean ADM2 level was higher in the patients with lymphovascular invasion and extrathyroidal extension than in patients without these conditions (Figure 6G). Interestingly, patients in the recurrent group had significantly higher ADM2 serum levels than those in the nonrecurrent group. The results of the human data indicate that ADM2 is strongly associated with obesity and tumour aggressiveness.

Discussion

This study attempted to identify the cell-autonomous, and noncell-autonomous factors and pathways that determine thyroid cancer progression using thyrocyte-specific $BRAF^{V600E}$-inducible mice fed an HFD. Thyroid tumour cells in thyrocyte-specific $BRAF^{V600E}$-inducible mice fed HFD showed dysmorphic follicular changes with mitochondrial ultrastructural alterations. ADM2 is a prominent secretory factor in tumour cells of HFD-fed thyrocyte-specific $BRAF^{V600E}$-inducible mice. Upregulation of ADM2 in tumour cells was enhanced by activation of the mitochondrial stress response pathway following fatty acid treatment *in vitro*. Furthermore, ADM2 expression is augmented in obese patients with thyroid cancer who show larger tumour size, a high prevalence of lymph node metastasis, and locoregional recurrence.

Kim *et al* have shown that $ThrbPV/PVPten^{+/-}$ mice with thyroid cancer developed by knock-in dominant-negative mutation of the thyroid hormone receptor β (*Thrb*) gene and deletion of one allele of the *Pten* gene harbour larger tumours with anaplastic phenotypes after being given an HFD [51]. They showed increased activation of JAK-STAT3 signalling pathways that may be activated by leptin, which originates from adipocytes in expanded fat pads with an HFD. This ($ThrbPV/PVPten^{+/-}$) is a representative example of an adipose tissue-adipokine-thyroid tumour connection in an animal model of thyroid cancer, which has the characteristic features of follicular thyroid cancer [51]. In this study, we did not validate the role of leptin-JAK-STAT3 activation in enhancing the expression of ADM2. However, the evidence strongly suggests that

thyroid tumour behaviour can be transformed into more progressive phenotypes with excessive high fat nutrition.

In the rat thyroid follicular cell line FRTL-5, *ADM2* increased by TSH [38]; however, in our model serum TSH levels remained unaltered by overnutrition compared with that in control mice (Figure 2E), suggesting that there were other factors inducing ADM2. Since we had previously identified the induction of mitokines by the ISR pathway [52–55], and as our electron microscopy data showed increased dysmorphic mitochondria, we hypothesised that ADM2 expression increased by ISR pathways. The transcription factor ATF4, which integrates cellular stresses, has been considered a major factor in stress-inducible ADM2 expression by regulating the ADM2 promoter [56]. Interestingly, secreted ADM2 plays a protective role in endoplasmic reticulum stress-induced myocardial injury through the PI3K–AKT signalling pathway [57]. These findings suggest that ADM2 may play a hormetic role in overcoming cellular stress under physiological and pathological conditions. Consistent with previous studies, we demonstrated that ADM2 expression increased with the activation of ATFs and DDIT3 in response to metabolic stresses, inducing mitochondrial inhibition (palmitic acid and rotenone), in thyroid cancer. Elevated levels of ADM2 in thyroid cancer may reduce the stress response; however, ADM2 plays a role in cancer progression.

In the TCGA database, *ADM2* was related to worse survival in total tumour and subtypes in relation to the presence of $BRAF^{V600E}$, although ADM2 decreased in tumour tissues compared with normal thyroid. These results indicate the tumour-specific role of ADM2 in regulating tumourigenesis independent of the BRAF mutation in thyroid cancer.

ADM2 was a predictor of survival in pancreatic cancer [42,43], and preoperative plasma ADM2 levels were identified as independent predictors of 5-year mortality, disease-free survival, and overall survival [43]. In addition, blocking ADM2 regulates ERK and Gli1–Bcl2 signalling, which are important for cell proliferation and survival in hepatocellular carcinoma [44]. Notably, increased ADM2 and decreased p-ERK levels were observed in healthy (noncancerous) thyroid glands in the HFD group (supplementary material, Figure S3). It is unclear whether ADM2 is directly involved in ERK phosphorylation in healthy thyroid glands; this might be a physiological difference due to the presence or absence of an oncogene. Nevertheless, we identified that ADM2 stimulates proliferation and migration by enhancing ERK signalling and is associated with aggressive clinicopathological factors in thyroid cancer.

As mentioned above, plasma and cellular levels of ADM2 are valuable prognostic markers in patients with cancer. However, the role of ADM2 in obese cancer patients has not yet been elucidated, and changes in the plasma and cellular levels of ADM2 have not yet been examined. We showed that ADM2 was increased in the thyroid of HFD-fed mice in both cancer and noncancer models (Figure 3 and supplementary material, Figure S3). Additionally, our results showed that blood ADM2 levels were increased when thyroid cancer was present with obesity as a comorbidity (Figure 6G and supplementary material, Table S2). Interestingly, whilst circulating ADM2 is inversely correlated with obesity in humans, ADM2 levels in adipose tissue are increased during obesity [58,59]. These findings demonstrate that circulating ADM2 originates from various tissues, including the thyroid gland, and is differentially regulated between physiological and pathological (cancerous) conditions. Therefore, we suggest that ADM2 may play a specific role as a biomarker for predicting the progression of thyroid cancer in obese patients.

Most of our evidence suggests a role for ADM2 in cancer cells; however, we have not yet been able to fully elucidate the effect of ADM2 on the vascular and immune systems. Although immune cell markers were not detected in the tumour of the mouse model (supplementary material, Figure S2), we found an association between *ADM2* and inflammatory response in TCGA-THCA data. ADM2 reduces organ injury (lung and kidney) and mortality by repairing vascular leakage and alleviating inflammatory responses, and alleviation of inflammatory response is accompanied by reduced macrophage infiltration [35]. In contrast to the septic condition, a reduced inflammatory response can be beneficial for tumour survival. However, in this study changes in immune cells could not be observed due to the limitations of the established mouse model.

In previous studies, we elucidated the roles of FGF21 and GDF15 as mitokines in thyroid cancer [54,60]. We found that serum FGF21 levels were associated with recurrence and BMI. Recombinant FGF21 induces epithelial-to-mesenchymal transition signalling in cancer cells and increases the migration of thyroid cancer cell lines [60]. Although *Fgf21*-related genes were not observed in BRAF-mutant mice fed HFD (Figure 3A), there is a possibility that increased serum FGF21 in obesity contributes to the progression of thyroid cancer. Interestingly, although ADM2 and GDF15 have common upstream regulators (*ATF*s and *CHOP*), the correlation result of TCGA-THCA shows that *ADM2* and *GDF15* were negatively correlated (supplementary material, Figure S5C). These results suggest that although ADM2 and GDF15 can be regulated as mitokines, their detailed roles and induction conditions may differ.

In conclusion, the present study shows the role of ADM2 in the nexus of obesity and thyroid cancer. It suggests the possibility of ADM2 as a therapeutic target in thyroid cancer and a useful biomarker for predicting thyroid tumour progression.

Acknowledgements

This research was supported by a grant from the Korea Health Technology R&D Project through the Korea Health Industry Development Institute, funded by the

Ministry of Health & Welfare, Republic of Korea (grant number: HR20C0025), and a National Research Foundation (NRF) of Korea grant funded by the Korean government (MEST) (grant number: 2019R1A2C1084125, 2021R1C1C1011183, and 2021R1A6A3A13046399). This work was supported by the Korean Endocrine Society of Hyangseol Young Investigator Award 2019 and Chungnam National University Hospital Research Fund, 2021.

Author contributions statement

JTK, KSK, YEK, BSK and MS made the concept and designed this study. JTK, MAL and SEL developed methodologies. HJK, HYK and JHL performed computational analysis. SMJ carried out electron microscopy and analysed data. JMK, HSS and SWC performed histology analysis. KHK measured hormone concentration. All authors were involved in writing the article and had final approval of the submitted article.

Data availability statement

The RNA sequencing data in this study have been deposited in the Gene Expression Omnibus (GEO). They are available with accession number GSE207666 (https://0-www-ncbi-nlm-nih-gov.brum.beds.ac.uk/geo/query/acc.cgi?acc=GSE207666).

References

1. Blüher M. Obesity: global epidemiology and pathogenesis. *Nat Rev Endocrinol* 2019; **15:** 288–298.
2. Chooi YC, Ding C, Magkos F. The epidemiology of obesity. *Metabolism* 2019; **92:** 6–10.
3. Jaacks LM, Vandevijvere S, Pan A, *et al*. The obesity transition: stages of the global epidemic. *Lancet Diabetes Endocrinol* 2019; **7:** 231–240.
4. Bardou M, Barkun AN, Martel M. Obesity and colorectal cancer. *Gut* 2013; **62:** 933–947.
5. Liu X, Sun Q, Hou H, *et al*. The association between BMI and kidney cancer risk: an updated dose-response meta-analysis in accordance with PRISMA guideline. *Medicine (Baltimore)* 2018; **97:** e12860.
6. Stolzenberg-Solomon RZ, Schairer C, Moore S, *et al*. Lifetime adiposity and risk of pancreatic cancer in the NIH-AARP Diet and Health Study cohort. *Am J Clin Nutr* 2013; **98:** 1057–1065.
7. Lee K, Kruper L, Dieli-Conwright CM, *et al*. The impact of obesity on breast cancer diagnosis and treatment. *Curr Oncol Rep* 2019; **21:** 41.
8. Onstad MA, Schmandt RE, Lu KH. Addressing the role of obesity in endometrial cancer risk, prevention, and treatment. *J Clin Oncol* 2016; **34:** 4225–4230.
9. Kim J, Gosnell JE, Roman SA. Geographic influences in the global rise of thyroid cancer. *Nat Rev Endocrinol* 2020; **16:** 17–29.
10. Kitahara CM, Pfeiffer RM, Sosa JA, *et al*. Impact of overweight and obesity on US papillary thyroid cancer incidence trends (1995-2015). *J Natl Cancer Inst* 2020; **112:** 810–817.
11. Cheong HS, Chang Y, Joo EJ, *et al*. Metabolic obesity phenotypes and risk of cellulitis: a cohort study. *J Clin Med* 2019; **8:** 953.
12. Son H, Lee H, Kang K, *et al*. The risk of thyroid cancer and obesity: a nationwide population-based study using the Korea National Health Insurance Corporation cohort database. *Surg Oncol* 2018; **27:** 166–171.
13. He Q, Sun H, Li F, *et al*. Obesity and risk of differentiated thyroid cancer: a large-scale case-control study. *Clin Endocrinol (Oxf)* 2019; **91:** 869–878.
14. Matrone A, Ferrari F, Santini F, *et al*. Obesity as a risk factor for thyroid cancer. *Curr Opin Endocrinol Diabetes Obes* 2020; **27:** 358–363.
15. Rahman ST, Pandeya N, Neale RE, *et al*. Obesity is associated with $BRAF^{V600E}$-mutated thyroid cancer. *Thyroid* 2020; **30:** 1518–1527.
16. Avgerinos KI, Spyrou N, Mantzoros CS, *et al*. Obesity and cancer risk: emerging biological mechanisms and perspectives. *Metabolism* 2019; **92:** 121–135.
17. Moschos SJ, Mantzoros CS. The role of the IGF system in cancer: from basic to clinical studies and clinical applications. *Oncology* 2002; **63:** 317–332.
18. Manzella L, Massimino M, Stella S, *et al*. Activation of the IGF axis in thyroid cancer: implications for tumorigenesis and treatment. *Int J Mol Sci* 2019; **20:** 3258.
19. Memmott RM, Dennis PA. Akt-dependent and -independent mechanisms of mTOR regulation in cancer. *Cell Signal* 2009; **21:** 656–664.
20. Berger NA. Obesity and cancer pathogenesis. *Ann N Y Acad Sci* 2014; **1311:** 57–76.
21. Rodríguez-Hernández H, Simental-Mendía LE, Rodríguez-Ramírez G, *et al*. Obesity and inflammation: epidemiology, risk factors, and markers of inflammation. *Int J Endocrinol* 2013; **2013:** 678159.
22. Pearson MJ, Herndler-Brandstetter D, Tariq MA, *et al*. IL-6 secretion in osteoarthritis patients is mediated by chondrocyte-synovial fibroblast cross-talk and is enhanced by obesity. *Sci Rep* 2017; **7:** 3451.
23. El-Wakkad A, El-Morsi Hassan N, Sibaii H, *et al*. Proinflammatory, anti-inflammatory cytokines and adiponkines in students with central obesity. *Cytokine* 2013; **61:** 682–687.
24. Xi C, Zhang GQ, Sun ZK, *et al*. Interleukins in thyroid cancer: from basic researches to applications in clinical practice. *Front Immunol* 2020; **11:** 1124.
25. Wu Q, Li B, Li Z, *et al*. Cancer-associated adipocytes: key players in breast cancer progression. *J Hematol Oncol* 2019; **12:** 95.
26. Bokobza E, Hinault C, Tiroille V, *et al*. The adipose tissue at the crosstalk between EDCs and cancer development. *Front Endocrinol (Lausanne)* 2021; **12:** 691658.
27. Laurent V, Toulet A, Attané C, *et al*. Periprostatic adipose tissue favors prostate cancer cell invasion in an obesity-dependent manner: role of oxidative stress. *Mol Cancer Res* 2019; **17:** 821–835.
28. Zhang T, Tseng C, Zhang Y, *et al*. CXCL1 mediates obesity-associated adipose stromal cell trafficking and function in the tumour microenvironment. *Nat Commun* 2016; **7:** 11674.
29. Huang M, Narita S, Inoue T, *et al*. Fatty acid binding protein 4 enhances prostate cancer progression by upregulating matrix metalloproteinases and stromal cell cytokine production. *Oncotarget* 2017; **8:** 111780–111794.
30. Weinberg JM. Lipotoxicity. *Kidney Int* 2006; **70:** 1560–1566.
31. Engin AB. What is lipotoxicity? *Adv Exp Med Biol* 2017; **960:** 197–220.
32. Lee MH, Lee JU, Joung KH, *et al*. Thyroid dysfunction associated with follicular cell steatosis in obese male mice and humans. *Endocrinology* 2015; **156:** 1181–1193.
33. Roh J, Chang CL, Bhalla A, *et al*. Intermedin is a calcitonin/calcitonin gene-related peptide family peptide acting through the calcitonin receptor-like receptor/receptor activity-modifying protein receptor complexes. *J Biol Chem* 2004; **279:** 7264–7274.

34. Zhang SY, Xu MJ, Wang X. Adrenomedullin 2/intermedin: a putative drug candidate for treatment of cardiometabolic diseases. *Br J Pharmacol* 2018; **175:** 1230–1240.
35. Xiao F, Wang D, Kong L, *et al*. Intermedin protects against sepsis by concurrently re-establishing the endothelial barrier and alleviating inflammatory responses. *Nat Commun* 2018; **9:** 2644.
36. Kitamura K, Kangawa K, Ichiki Y, *et al*. Adrenomedullin: a novel hypotensive peptide identified in human Pheochromocytoma. *Hypertension* 1993; **22:** 448.
37. Li L, Ma P, Liu Y, *et al*. Intermedin attenuates LPS-induced inflammation in the rat testis. *PLoS One* 2013; **8:** e65278.
38. Nagasaki S, Fukui M, Asano S, *et al*. Induction of adrenomedullin 2/-intermedin expression by thyroid stimulating hormone in thyroid. *Mol Cell Endocrinol* 2014; **395:** 32–40.
39. Che CL, Zhang YM, Zhang HH, *et al*. DNA microarray reveals different pathways responding to paclitaxel and docetaxel in non-small cell lung cancer cell line. *Int J Clin Exp Pathol* 2013; **6:** 1538–1548.
40. Lin Chang C, Roh J, Park JI, *et al*. Intermedin functions as a pituitary paracrine factor regulating prolactin release. *Mol Endocrinol* 2005; **19:** 2824–2838.
41. Pfeil U, Aslam M, Paddenberg R, *et al*. Intermedin/adrenomedullin-2 is a hypoxia-induced endothelial peptide that stabilizes pulmonary microvascular permeability. *Am J Physiol Lung Cell Mol Physiol* 2009; **297:** L837–L845.
42. Hollander LL, Guo X, Salem RR, *et al*. The novel tumor angiogenic factor, adrenomedullin-2, predicts survival in pancreatic adenocarcinoma. *J Surg Res* 2015; **197:** 219–224.
43. Lu YM, Zhong JB, Wang HY, *et al*. The prognostic value of intermedin in patients with breast cancer. *Dis Markers* 2015; **2015:** 862158.
44. Guo X, Schmitz JC, Kenney BC, *et al*. Intermedin is overexpressed in hepatocellular carcinoma and regulates cell proliferation and survival. *Cancer Sci* 2012; **103:** 1474–1480.
45. Davies H, Bignell GR, Cox C, *et al*. Mutations of the BRAF gene in human cancer. *Nature* 2002; **417:** 949–954.
46. Undeutsch H, Löf C, Offermanns S, *et al*. A mouse model with tamoxifen-inducible thyrocyte-specific cre recombinase activity. *Genesis* 2014; **52:** 333–340.
47. Franco AT, Malaguarnera R, Refetoff S, *et al*. Thyrotrophin receptor signaling dependence of Braf-induced thyroid tumor initiation in mice. *Proc Natl Acad Sci U S A* 2011; **108:** 1615–1620.
48. Väremo L, Nielsen J, Nookaew I. Enriching the gene set analysis of genome-wide data by incorporating directionality of gene expression and combining statistical hypotheses and methods. *Nucleic Acids Res* 2013; **41:** 4378–4391.
49. Love MI, Huber W, Anders S. Moderated estimation of fold change and dispersion for RNA-seq data with DESeq2. *Genome Biol* 2014; **15:** 550.
50. Korbecki J, Bajdak-Rusinek K. The effect of palmitic acid on inflammatory response in macrophages: an overview of molecular mechanisms. *Inflamm Res* 2019; **68:** 915–932.
51. Kim WG, Park JW, Willingham MC, *et al*. Diet-induced obesity increases tumor growth and promotes anaplastic change in thyroid cancer in a mouse model. *Endocrinology* 2013; **154:** 2936–2947.
52. Choi MJ, Jung SB, Lee SE, *et al*. An adipocyte-specific defect in oxidative phosphorylation increases systemic energy expenditure and protects against diet-induced obesity in mouse models. *Diabetologia* 2020; **63:** 837–852.
53. Kang SG, Choi MJ, Jung SB, *et al*. Differential roles of GDF15 and FGF21 in systemic metabolic adaptation to the mitochondrial integrated stress response. *iScience* 2021; **24:** 102181.
54. Kang YE, Kim JM, Lim MA, *et al*. Growth differentiation factor 15 is a cancer cell-induced mitokine that primes thyroid cancer cells for invasiveness. *Thyroid* 2021; **31:** 772–786.
55. Jung SB, Choi MJ, Ryu D, *et al*. Reduced oxidative capacity in macrophages results in systemic insulin resistance. *Nat Commun* 2018; **9:** 1551.
56. Kovaleva IE, Garaeva AA, Chumakov PM, *et al*. Intermedin/adrenomedullin 2 is a stress-inducible gene controlled by activating transcription factor 4. *Gene* 2016; **590:** 177–185.
57. Teng X, Song J, Zhang G, *et al*. Inhibition of endoplasmic reticulum stress by intermedin(1-53) protects against myocardial injury through a PI3 kinase-Akt signaling pathway. *J Mol Med (Berl)* 2011; **89:** 1195–1205.
58. Kim J, Lee SK, Kim D, *et al*. Altered expression of adrenomedullin 2 and its receptor in the adipose tissue of obese patients. *J Clin Endocrinol Metab* 2020; **105:** dgz066.
59. Lv Y, Zhang SY, Liang X, *et al*. Adrenomedullin 2 enhances Beiging in white adipose tissue directly in an adipocyte-autonomous manner and indirectly through activation of M2 macrophages. *J Biol Chem* 2016; **291:** 23390–23402.
60. Kang YE, Kim JT, Lim MA, *et al*. Association between circulating fibroblast growth factor 21 and aggressiveness in thyroid cancer. *Cancers (Basel)* 2019; **11:** 1154.

SUPPLEMENTARY MATERIAL ONLINE

Supplementary materials and methods

Figure S1. Diet-induced obesity causes cancer proliferation in *LSL-Braf*^{V600E};*Tg*CreER^{T2} mice

Figure S2. Expression of immune cell marker (CD4, CD8, and CD163) in *LSL-Braf*^{V600E};*Tg*CreER^{T2} mice fed CD and fed HFD

Figure S3. The effects of diet-induced obesity on thyroid weight and ADM2 expression in *LSL-Braf*^{V600E} mice

Figure S4. Expression of *ADM2* and ISR genes (GTEx and TCGA)

Figure S5. Survival analysis in subgroups and correlation between mitokines in TCGA-THCA dataset

Figure S6. KEGG mapper using differentially expressed genes of RNAseq result from TCGA-THCA between the top 25% group and the bottom 25% group (the group with low *ADM2* expression) were classified according to the *ADM2* expression

Figure S7. Immunohistochemistry for ADM2 in the thyroid gland of papillary thyroid cancer patients

Table S1. Relationship between ADM2 staining intensity and clinicopathological factors in patients with papillary thyroid cancer (PTC)

Table S2. Comparison of clinicopathological findings in relation to circulating ADM2 (median value) in participants with papillary thyroid cancer (PTC) ($n = 108$)